Ingeniería, investigación y tecnología
ISSN: 1405-7743
Universidad Nacional Autónoma de México, Facultad de Ingeniería

Aragon-Verduzco, David Antonio; Escarela-Perez, Rafael; Olivares-Galvan, Juan Carlos; Campero-Littlewood, Eduardo; Maximov, Serguei; Hernández-Ávila, Jose Luis

Numerical simulation of a squirrel cage motor including magnetic wedges and radial vents
Ingeniería, investigación y tecnología, vol. XXII, no. 4, e1840, 2021, October-December
Universidad Nacional Autónoma de México, Facultad de Ingeniería

DOI: https://doi.org/10.14482/INDES.30.1.303.661

Available in: https://www.redalyc.org/articulo.oa?id=40471804005

Ingeniería Investigación y Tecnología
volumen XXII (número 4), octubre-diciembre 2021 1-10
ISSN 2594-0732 FI-UNAM artículo arbitrado
Información del artículo: Recibido: 15 de noviembre de 2020, aceptado: 29 de mayo de 2021.

https://doi.org/10.22201/fi.25940732e.2021.22.4.025

Ingeniería Investigación y Tecnología

Numerical simulation of a squirrel cage motor including magnetic wedges and radial vents

Simulación numérica de un motor jaula de ardilla que incluye cuñas magnéticas y ventilaciones radiales

Aragon-Verduzco David Antonio
Universidad Autónoma Metropolitana, Unidad Lerma
Departamento de Procesos Productivos
E-mail: david.aragon344@gmail.com
https://orcid.org/0000-0002-6791-1322

Escarela-Perez Rafael
Universidad Autónoma Metropolitana, Unidad Azcapotzalco
Departamento de Energía
E-mail: r.escarela@ieee.org
https://orcid.org/0000-0001-7415-3059

Olivares-Galvan Juan Carlos
Universidad Autónoma Metropolitana, Unidad Azcapotzalco
Departamento de Energía
E-mail: jolivaresgalvan@gmail.com
https://orcid.org/0000-0002-1935-2669

Campero-Littlewood Eduardo
Universidad Autónoma Metropolitana, Unidad Azcapotzalco
Departamento de Energía
E-mail: ecl@azc.uam.mx
https://orcid.org/0000-0003-1708-1532

Maximov Serguei
Instituto Tecnológico de Morelia
Tecnológico Nacional de México
Programa de Graduados e Investigación en Ingeniería Eléctrica
E-mail: sgmaximov@yahoo.com.mx
https://orcid.org/0000-0002-2144-9208

Hernández-Ávila Jose Luis
Universidad Autónoma Metropolitana. Unidad Azcapotzalco
Departamento de Energía
E-mail: hajl@correo.azc.uam.mx
https://orcid.org/0000-0002-5691-9329

Abstract

This work is a proposal of a finite element model to obtain the electromagnetic performance of a squirrel cage motor considering the magnetic wedges and radial vents. To analyze the electromagnetic performance at the design stage, without the need to build a prototype, the paper proposes a simple two dimensions finite element model, which includes components as magnetic wedges used to hold the windings in the stator slots, radial vents in the core, which are part of motor cooling system, and edge effects to improve the model. The stator and rotor cores are modeled with an equivalent homogeneous permeability, obtained from the combination of the radial air vents of rotor and stator and the magnetic core material. The permeability of magnetic wedges is also considered. Edge effects considered are the end winding leakage inductance, representing the leakage flux in the end coils of the stator, and an equivalent impedance between rotor bars due to conductivity and leakage flux in the rings of the squirrel cage. The results obtained are compared with experimental tests performed in steady state to validate the model. Furthermore, no-load and blocked-rotor tests are simulated to estimate the equivalent circuit parameters and draw the typical induction motor torque-speed curve, which is compared with the obtained curve by means of Thevenin's theorem. With this proposed model, the results are close to the ones obtained experimentally. The implementation of a 3D model is complex, and the computational cost can be much higher, compared to the 2D model developed here.
Keywords: Electromagnetic performance, numerical simulation, squirrel cage motor, magnetic wedges, radial vents.

Resumen

Este trabajo es una propuesta de un modelo de elementos finitos para obtener el desempeño electromagnético de un motor jaula de ardilla que cuenta con cuñas magnéticas y ventilaciones radiales. Para el análisis del desempeño electromagnético, en la etapa de diseño, evitando la necesidad de construir un prototipo, se propone un modelo simple de elementos finitos en dos dimensiones que incluye componentes como cuñas magnéticas utilizadas para mantener los devanados en las ranuras del estator, ventilaciones radiales en el núcleo, que son parte del sistema de enfriamiento del motor, y efectos de borde para complementar el modelo. Los núcleos del estator y del rotor se modelan con una permeabilidad homogénea equivalente, obtenida de la combinación de las salidas de aire radiales del rotor y el estator y material del núcleo magnético. También se considera la permeabilidad de las cuñas magnéticas. Los efectos de borde que se consideran son: la inductancia de dispersión en el cabezal del devanado, el cual representa el flujo disperso al final de las bobinas del estator, y una impedancia equivalente entre las barras del rotor debido a la conductividad y el flujo disperso en los anillos de la jaula de ardilla. Para validar el modelo, los resultados obtenidos se comparan con pruebas experimentales realizadas en estado estable. Adicionalmente, las pruebas de rotor bloqueado y sin carga se simulan para estimar los parámetros del circuito equivalente y obtener la curva par-velocidad del motor inducción, la cual se compara con la curva obtenida mediante el teorema de Thévenin. Los resultados del modelo propuesto son cercanos a los obtenidos en el laboratorio. La implementación de un modelo 3D es compleja y el costo computacional puede ser alto comparado con el modelo 2D desarrollado en este trabajo.
Descriptores: Desempeño electromagnético, simulación numérica, motor jaula de ardilla, cuñas magnéticas, ventilaciones radiales.

https://doi.org/10.22201/fi.25940732e.2021.22.4.025

Introduction

The electromagnetic characteristics of the squirrel cage motor make it the most used prime mover in industry. Methods to estimate motor performance, like equivalent circuits, analytical or numerical representation, are used and techniques to compute some electrical parameters as genetic algorithm and differential evolution are examples of different tools. In any case, it is important to analyse the design and to determine the performance and the motor parameters before manufacture.

Maxwell's equations describe the relationship between electromagnetic variables enabling the temporal and spatial analysis in energy conversion devices. However, due to the motor geometry and the non-linear characteristics of materials, the analysis and design using analytical methods is not an easy task.

The Finite Element Method (FEM) is a tool of great help to solve systems of differential equations in many areas (Castañeda *et al.,* 2020). The essential idea of FEM is to geometrically divide a domain or a body in small subdivisions or elements that are joined by nodes and form an assembly called mesh. The task is to postulate simple equations and assemble the information that comes from each element generating an algebraic system of equations to get the solution of the proposed model.

The study of electromagnetic devices with FEM gives a very close representation of their steady state (Guzman *et al.,* 2015) and transient (Qiu *et al.,* 2020) behaviour. It also helps to visualize and obtain the distribution of magnetic flux density, leakage flux, magnetic field strength, among other variables.

This work includes design elements that have been considered by researchers to tackle different problems. The examined elements are: the pack of ferromagnetic laminations with radial ventilation channels in rotor and stator (Cha *et al.,* 2017; Tong *et al.,* 2018), the magnetic wedges to close slots of the stator pack (Frosini & Pastura, 2020; Yang *et al.,* 2020; Verucchi *et al.,* 2017), the edge effects of the stator winding and of the rotor rings that short-circuited the squirrel cage bars (Jimenez *et al.,* 2016; Kumar *et al.,* 2020). These elements of the squirrel cage motor are all included in the simple 2D FEM model proposed in this paper.

The motivation of this work is to have a methodology to obtain the parameters and simulate the behaviour of large squirrel cage motors (medium and high voltage) using FEM in the design phase, before performing the usual electrical laboratory tests determined by international standards (IEC, 2007; IEEE, 2004). Experimental tests can represent a high mechanical stress and an increase of the motor temperature. In addition, there must be a high level of safety to avoid damage to the motor and to not affect the security of the personnel that performs the tests.

The paper is organized in the following manner. Section 2 gives a brief description of the squirrel cage motor, the equivalent circuit and the elements included in the FEM model. In Section 3, the FEM applied to electromagnetism is presented. Section 4 shows a simple 2D model. Section 5, the electrical characteristics, geometry, boundary conditions and the electromagnetic field periodicity in the motor for the 2D model are commented. In Section 6 several simulations are performed and in order to verify the obtained results are compared with the laboratory tests and finally, section 7 the conclusion of the paper.

Squirrel cage motor

The squirrel cage motor is a device that uses electromagnetic fields to convert electrical energy into mechanical. The stator has a laminated ferromagnetic core with slots where windings are placed and fed with three-phase voltages. The rotor has a squirrel-cage inserted in its slots. The cores are normally constructed with non-grain-oriented silicon steel.

When the motor is loaded, the three phase stator currents produce a magnetic field that rotates at synchronous speed *(N_s)*. The mechanical rotor speed lags the rotating magnetic field and produces a slip *(s)* proportional to the percentage of the relative speed between synchronous and mechanical speed *(Nm)*. The frequency of the voltages induced in the rotor winding or bars is called "slip frequency", denoted by f_r, obtained by the product of the slip and the stator frequency f_e:

$$f_r = s \cdot f_e \tag{1}$$

Figure 1 shows the steady-state equivalent circuit of the squirrel cage motor. The resistances of stator (R1), rotor (R'2) and the equivalent resistance to magnetic loss (Rc) and the inductances of stator (L1), rotor (L'2) and magnetization (Lm) are the parameters that represent the presence of electromagnetic field linkages and current in conductors. V1 represents the phase voltage.

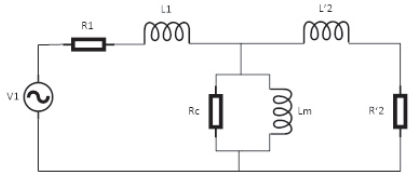

Figure 1. Single-phase equivalent circuit (referred to the stator) of a balanced three-phase squirrel cage motor

The proposed method relates the physical variables of the motor with the equivalent circuit parameters. It uses the FEM to calculate the circuit parameters as well as the equivalent circuit currents.

Radial rotor and stator ventilation ducts

In the FEM, the consideration of the complete geometry of a structure demands expensive computational resources. For this reason, it is convenient to simplify the motor structure. In the case of laminated magnetic cores, the shape of the magnetic sheets and the air between sheets may cause numerical problems, since there is a strong dimensional disproportion between the length of the magnetic core and the thickness of the sheets.

One solution is to model an equivalent macroscopic structure using a homogenization technique, this technique allows simplifying the behavior of a material. Starting from a heterogeneous structure that consists of several materials and can be determined in a homogeneous equivalent structure. This technique requires the use of the magnetic circuit concept.

The geometry of the radial package and vents of the stator and rotor is shown in Figure 2a. The homogeneous permeability is calculated considering a Cartesian system and assuming that the magnetic flux is in the "y" direction. The reluctance presented by the system is a parallel combination of the reluctances of the stack and the radial vents. This is shown in Figure 2b (Salon & Chari, 1999), where:

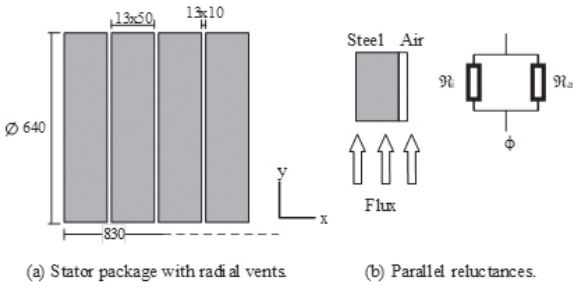

(a) Stator package with radial vents. (b) Parallel reluctances.

Figure 2. Equivalent homogeneous permeability of laminated stack (dimensions in mm)

$\Re_i$ = the silicon steel laminated core reluctance
$\Re_a$ = the air reluctance
φ = the flux

The reluctance values for air (a) and silicon steel laminated core (i) are:

$$\Re_a = r / \mu_0 b_a \quad (2)$$

$$\Re_i = r / \mu_i b_i \quad (3)$$

Where:

r = radial longitude
b = stack axial length
μ_i and μ_0 = the permeability of silicon steel laminated core and air, respectively

Thus, the equivalent permeability (μ_{eq}) being:

$$\mu_{eq} = \mu_i bi + \mu_0 b_a / b_i + b_a \quad (4)$$

It can be seen that as the rotor ducts and the stack have the same length (this is also valid for the stator) the equivalent permeability changes depend only on the magnetic permeability.

Magnetic materials in the core

The stator and rotor cores of squirrel cage motors are manufactured with lamination thicknesses of 0.27 to 0.65 mm to avoid eddy or circulating currents. The ferromagnetic laminations are mainly made with iron and alloys, since they offer a better cost-benefit of motor performance. These materials are known as electrical steels, since they are highly permeable. Investigations carried out showed that to improve the electrical characteristics of the steels, around 0.6 % to 3 % of silicon is added and thermal treatments such as annealing and recrystallization are made in order to reduce power losses (eddy and hysteresis) (Liu *et al.*, 2015).

Furthermore, magnetic wedges located in the slots of the stator core are used to improve the performance characteristics, providing a magnetic path that closes the slots and reduces the air gap. Core losses decrease under no load condition and reduce the harmonic content in the spatial distribution of the magnetic flux. It also helps to keep the coils in the slots, particularly during motor starting due to the electrodynamic forces (Verucchi *et al.*, 2017). The magnetic wedge is shown in Figure 3 and its composition is often a mixture of powder iron and a thermosetting resin.

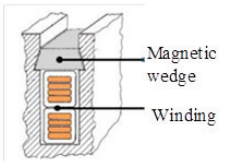

Figure 3. Magnetic wedge

The magnetic B-H characteristic of the core material, as well as the obtained equivalent permeability and the magnetic wedge permeability are shown in Figure 4.

https://doi.org/10.22201/fi.25940732e.2021.22.4.025

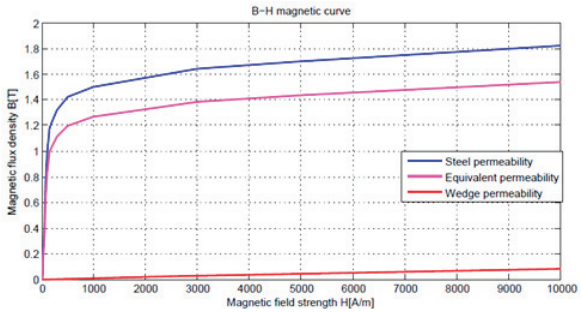

Figure 4. B-H curve of the motor magnetic materials

Edge effects

To have a better representation of the squirrel cage motor performance, it is important to consider the leakage flux due to the overhang winding at the end of the magnetic steel pack (Figure 5). To obtain the total leakage flux, it is necessary to determine some parameters such as starting torque, starting current and power factor, among others (Schuhmann *et al.*, 2013).

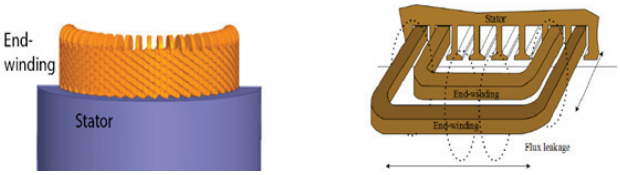

a) End-winding in the stator b) Leakage flux due stator end-windings
Figure 5. Edge effects considered in the FEM model

The solid conductors or bars of the squirrel-cage rotor are short-circuited with end-rings that have a finite impedance between each bar (Figure 6) (Escarela *et al.*, 2009). The inductance (L_{er}) basically depending on the geometry of the short-circuit end-rings and the resistance (R_{er}) depending on the resistivity of the squirrel cage material and the dimensions of the end rings (Wang *et al.*, 2014).

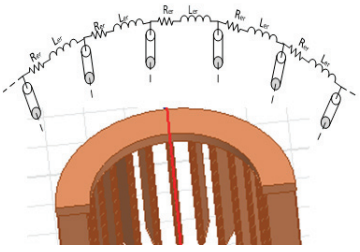
Figure 6. Equivalent circuits representing the squirrel-cage

There is technical literature (Pyrhonen, 2013) and (Boldea, 2020) that describes how to determine the end winding leakage inductance and to determine the end ring impedance parameters, which are an extension of the model of the stator winding and of the end ring squirrel cage.

Finite element method applied to low-frequency electromagnetism

In electromagnetism, the Maxwell's equations for electric and magnetic fields are expressed as follows:

$$\nabla \times \boldsymbol{E} = -\partial \boldsymbol{B} / \partial t$$

$$\nabla \times \boldsymbol{H} = J + \partial \boldsymbol{D} / \partial t \quad (5)$$

$$\nabla \cdot \boldsymbol{B} = 0$$

Where:

$\boldsymbol{E}$ = Vector of electric field strength
$\boldsymbol{B}$ = Vector of magnetic induction
$\boldsymbol{H}$ = Vector of magnetic field intensity
$\boldsymbol{D}$ = Vector of electric displacement or electric induction
$\boldsymbol{J}$ = Vector of electric current density

Maxwell's equations are complemented with the constitutive relations that establish the characteristics of the medium: The presence of nonlinearities, remaining inductions, and the behaviour of the fields in the interface between different media, among others.

$$\boldsymbol{D} = \varepsilon \boldsymbol{E}$$
$$\boldsymbol{B} = \mu \boldsymbol{H} \quad (6)$$
$$\boldsymbol{J} = \sigma \boldsymbol{E}$$

Where:

ε = Electrical permittivity
σ = Electric conductivity
μ = Magnetic permeability

In this work, all media are considered isotropic.

There are equivalent formulations, based on vector and scalar, magnetic and electric potentials to implicitly solve the Maxwell's equations. The solution of the differential equations in partial derivatives, in terms of the potentials, represent the solution of the Maxwell's equations. In this problem, the displacement current is negligible as compared to the main current for low frequency operation and therefore it can be omitted (Bastos & Sadowski, 2003).

$$[\partial \boldsymbol{D} / \partial t << \boldsymbol{J}] \Rightarrow \nabla \times \boldsymbol{H} \simeq \boldsymbol{J} \quad (7)$$

In this case, the formulation used is the magnetic vector potential (***A***), and the electric scalar potential (***V***), formulation $A - V$, which leads to a simple 2D way to establish the coupling between electrical circuits and the magnetic field equations in the induction machine:

$$\nabla \times (1/\mu \nabla \times \boldsymbol{A}) + \sigma [\partial \boldsymbol{A}/\partial t + \nabla V] = 0 \tag{8}$$

Simple 2D model

The squirrel cage motors have intricate geometries that require a detailed analysis. Research performed in (Pechlivanidou *et al.*, 2019; Fireţeanu *et al.*, 2019) compares 2D and 3D FEM models showing the differences in the results. Substantially 3D models require much more computing time than 2D models and the size of the files used in 3D analyses is 10 times greater than the 2D analyses files. The results of both techniques have a percentage error that seems to be significant only for a few electromagnetic quantities, like the torque and the air-gap total flux density where the error is around 8 % between 2D and 3D analyses. A simple 2D model is proposed to reduce the computing time, simplify the problem, and accomplish a detailed representation of the geometry. Hence, the magnetic vector potential and the current density have only one component in the axial direction (z) of the machine (Bastos & Sadowski, 2003), such that:

$$\boldsymbol{A} = A\,(x,y)\,\boldsymbol{k}$$
$$\boldsymbol{J} = J\,(x,y)\,\boldsymbol{k} \tag{9}$$

Where $\boldsymbol{k}$ is the unit vector in the z direction. With this consideration, the equation (8) can be written in Cartesian coordinates as:

$$\frac{\partial}{\partial x}\left[\frac{1}{\mu}\frac{\partial A_z}{\partial x}\right]+\frac{\partial}{\partial y}\left[\frac{1}{\mu}\frac{\partial A_z}{\partial y}\right]=\sigma\frac{\partial A_z}{\partial t}+\sigma\nabla V \tag{10}$$

Equations for conductors

Two types of conductors, of different dimensions, are considered in this work: Solid conductors that, due to their large dimensions and the skin effect, do not have a uniform distribution of the current in their cross-section and the filamentary conductors in the winding coils where the current is considered uniformly distributed.

Solid conductors: By modifying equation (10) for solid conductors we get the following relation:

$$\frac{\partial}{\partial x}\left[\frac{1}{\mu}\frac{\partial A_z}{\partial x}\right]+\frac{\partial}{\partial y}\left[\frac{1}{\mu}\frac{\partial A_z}{\partial y}\right]-\sigma\frac{\partial A_z}{\partial t}+\sigma\frac{V_m}{\Gamma}=0 \tag{11}$$

$$V_m = R_m I_m + R_m \int_S \sigma \frac{\partial A}{\partial t} dS \tag{12}$$

Where:

V_m = the potential difference between the conductor terminals
R_m = the DC resistance of the conductor
I_m = the total current in the conductor
S = the cross-section of the conductor
Γ = the length of the conductor

Figure 7 shows the solid conductor.

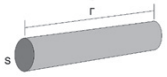

Figure 7. Solid conductor

Filamentary conductors: Let Γ be the length, I_f the current and N_c the number of turns. The conductor has a small cross-section (s) so as to avoid the skin effect. Figure 8 shows the filamentary conductor.

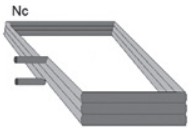

Figure 8. Filamentary conductors

Similarly, as it was for solid conductors, the equation (10), for filamentary conductors is:

$$\frac{\partial}{\partial x}\left[\frac{1}{\mu}\frac{\partial A_z}{\partial x}\right]+\frac{\partial}{\partial y}\left[\frac{1}{\mu}\frac{\partial A_z}{\partial y}\right]-\sigma\frac{\partial A_z}{\partial t}+\sigma\frac{V_f}{\Gamma}=0 \tag{13}$$

$$V_f = R_f I_f + N_c \Gamma \frac{\partial A_z}{\partial t} \tag{14}$$

Finally, the system of equations for the analysis of low frequency electromagnetic problem is as follows:

$$\nabla\times\left(\frac{1}{\mu}\nabla\times A_z\right)+\sigma\frac{\partial A_z}{\partial t}=\frac{\sigma}{\Gamma}V_z \tag{15}$$

$$V_m = R_m I_m + R_m \int_s \sigma \frac{\partial A_z}{\partial t} dS \tag{16}$$

$$V_f = R_f I_f + L\frac{dI_f}{dt} + N\Gamma\frac{\partial A_z}{\partial t} \quad (17)$$

An additional term has been introduced in (17): $L\, dI_f / dt$, to take into account the leakage flux in the end-windings, shown in Figure 5.

SQUIRREL CAGE MOTOR MODELING

This section presents the finite element model of a squirrel cage motor. The considered model assumptions are:

1. Three-dimensional effects are incorporated using a 2D model of the electromagnetic system complemented with resistances and inductances representing those effects.
2. In a simple 2D model, an isotropic media is assumed, but nonlinear, which means that the saturation phenomenon is considered.
3. The dielectric and conductive characteristics are linear, therefore, the permittivity of the material ($\in$) and the conductivity (σ) are constants.

MAIN SPECIFICATIONS OF SIMULATED MOTOR

Table 1. Specifications of the motor

Motor type	Three phases
Rated power, P_n	1400 hp
Nominal supply voltage, V_{fn}	7200 V (Line voltage)
Connection type	Star
Electrical frequency, f_e	60 Hz
Length of the stator and rotor magnetic core	830 mm
External diameter of the stator magnetic core	690 mm
Internal diameter of the stator	420 mm
Length of the air gap	2.4 mm
Pole pairs number	2
Number of stator sots	48
Number of rotor sots	58
Parallel branches	2
Turns in series in a stator coil	8
Stator slot pitch	12

SLOTS DIMENSIONS

Figure 9 shows the stator and rotor slots with their dimensions.

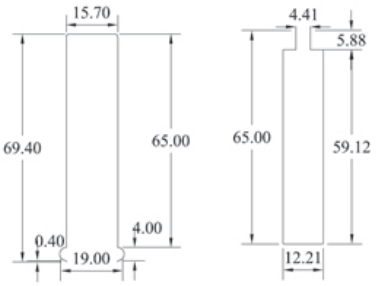

Figure 9. Stator and rotor slots dimensions (mm)

PERIODICITY AND BOUNDARY CONDITIONS

In the studied motor, it is used a periodicity condition due to its symmetry that delimits the boundaries of periodic portions with equal potential values, and to solve equation (10), boundary conditions must be considered. The boundaries that define the selected domain are the stator core outer periphery and the rotor core inner periphery. The evaluation of the electromagnetic field in all FEM simulations considers the magnetic vector potential A_z as unknown in the whole domain. The Dirichlet condition is considered in this boundary as no magnetic flux is crossing it: $A_z = A_0 = 0$.

SIMULATIONS RESULTS

The simulations presented in this work result from a time-harmonic analysis performed in a commercial FEM software (Altair, 2016) at constant slip values (rotor speed constant values) and do not consider the movement of the rotor with respect to the stator. It is important to point out that the results do not depend on FEM software used, the important thing is to considerer the characteristics mentioned in this paper to obtain accurate results close to the real motor.

The frequency in the rotor circuit is adjusted according to equation (1). In Figure 10 the results are shown graphically for a complete speed range.

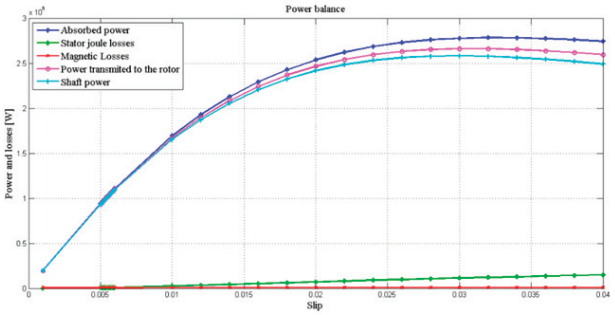

Figure 10. Curve of the power balance

Full load simulation

These simulations contain the motor characteristics for a steady-state operation. In Table 2, electrical parameters as the nominal current (I1n), nominal rotation (nn), nominal slip (sn), nominal torque (Th) and nominal power factor (cosθn) are presented and the results show a good accuracy (less than 1.2 % relative error) between the simulations and the laboratory values.

Table 2. Comparison of values obtained from simulation and laboratory data

Parameters	I1n (A)	nn (rpm)	sn	Tn (Nm)	cosθn
Simulation values	99.0	1789.7	0.0057	5590	0.86
Laboratory values	99.8	1789.6	0.00577	5597	0.87
Percent relative error	0.8	0.005	1.2	0.12	1.1

In Table 3, the power balance in the squirrel cage motor motor is shown. Specifically, the electrical input (P1n), Joule losses in stator winding (Pj1n), core loss (Pmn), Joule losses in rotor winding (Pj2n) and efficiency (ηn) are presented. In almost all the calculated values, the obtained relative error is low (less than 1.7 %). Only for the case of core losses the relative error was 4.16 %, in this work the Berttoti formula (Bertotti, 1998) was used to calculate them.

Figure 11 shows the lines of the magnetic field forming two poles. The machine under study is a 4 pole (for symmetry only two poles are shown).

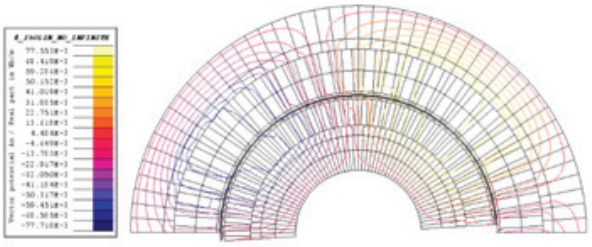

Figure 11. Magnetic field lines for the steady-state operation of the machine with rated load (s=0.0057)

Blocked-rotor simulation

The blocked rotor operation is simulated with a slip s=1 and the motor is supplied with a reduced voltage from 15 % to 30 % of the nominal value. For the rated current 98.4 A, an applied voltage of 866 V corresponds to an active power of 30747 W.

The distribution of the magnetic field density can be seen in Figure 12. As the slip is equal to one, the frequency of the rotor is the same as the frequency of the source. Therefore, the skin effect in the rotor bars is more pronounced in this condition than when it operates at full load.

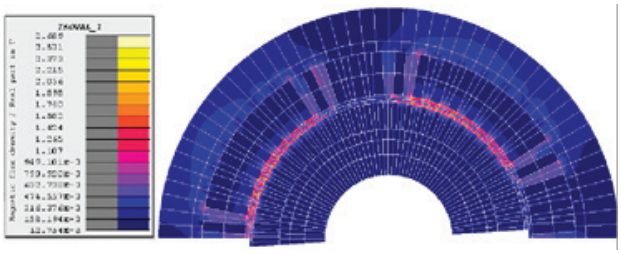

Figure 12. Magnetic flux density operating at locked rotor (s=1.0)

In Figure 13, the current density in the bars is shown. As the currents are induced in the rotor bars, a secondary magnetic field is produced which opposes the primary magnetic field due to the skin effect.

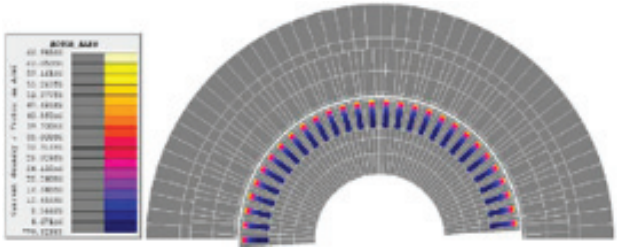

Figure 13. Density of current in the rotor bars at locked rotor (s=1.0)

No-load simulation

The simulation at no-load is performed with *s*=0.001, since it represents a slip value much less than the nominal slip. The objective of this simulation is to calculate

Table 3. Comparison of values obtained from simulation and laboratory data

Parameters	P1n (W)	Pj1n (W)	Pmn (W)	P2n (W)	ηn (%)
Simulation values	1074853	9596	11000	1045589	97.56
Laboratory values	1087580	9700	10560	1044180	96.01
Percent relative error	1.17	1.07	4.16	0.13	1.61

the currents at no-load, when the motor is fed at nominal voltage. For a slip value s=0.001 at no-load the stator current corresponds to I_{oc}=34.7A and the value of the power loss in the magnetic core is P_{oc}=11,111 W.

Calculation of the parameters of single−phase equivalent circuit of the three-phase squirrel cage motor

The equivalent circuit parameters of the motor are calculated from the results of simulations at no-load and blocked rotor (Umans, 2014). From the simulation of the motor operation at no-load, the magnetization reactance and the equivalent resistance due to the losses in the iron can be calculated. From the locked rotor simulation, the rotor resistance and the leakage inductance referred to the stator are obtained.

Table 4 presents the values of the parameters of the equivalent circuit of the modelled induction machine.

Table 4. Equivalent circuit parameters of the simulated induction machine

Parameters	R1 (Ω)	L1 (mH)	Rc (kΩ)	Lm (mH)	R′2 (Ω)	L′2 (mH)
Values	0.33	11.6	4.67	318	0.73	11.64

Since the parameters that were obtained from the simulations performed by the FEM (Table 4) and the analysis of Thevenin's theorem applied to the equivalent circuit of the induction machine (Umans, 2014), the obtained speed-torque curves are shown in Figure 14

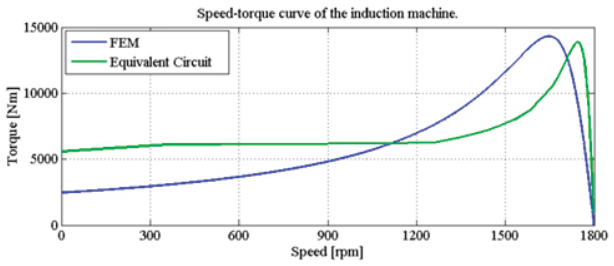

Figure 14. Speed-torque curve

In Figure 14 it can be observed an appreciable difference between electromagnetic torque obtained by FEM and with the equivalent circuit. This is mainly due to the fact that the curve obtained with the FEM considers the non-linearity of magnetic materials and does not neglect the effects of eddy currents.

Thevenin's theorem can be used to calculate some values of the motor starting parameters such as the electromechanical torque and the starting current. However, in order to obtain more precise parameters values, that actually catch the start-up phenomenon, authors suggest performing a transitory analysis.

Conclusion

This paper provides a model of a three-phase squirrel cage motor of 1400 hp using the finite element method. Several simulations were carried out at the frequency domain which made possible to obtain the accurate electromagnetic performance and reliable parameters of the motor equivalent circuit. In the proposed quasi-3D FEM model important physical aspects such as radial ventilation ducts, magnetic wedges and edge effects of the machine were considered. Periodicity and boundary conditions were also selected keeping in view the efficiency of the program.

The theory behind the method was developed using a deep analysis of the electromagnetic equations that made possible to perform the modelling of the squirrel cage motor. Using valid assumptions, a formulation with the vector magnetic potential was obtained (non-linear diffusion equation). In principle, this equation cannot be solved directly since it has two unknowns: the vector magnetic potential and the scalar electric potential. However, to obtain the scalar electric potential, the equations of the massive and filamentary conductors were used that allow the interconnection with external devices, thus solving a circuit-field problem.

The analysis performed includes a complete overview of the input-output variables of a squirrel cage motor as well as the equivalent circuit parameters, i.e. voltages and currents in stator and rotor. Also, internal variables, such as the magnetic field and the magnetic field density are obtained at different operation characteristics and using a shorter computing time than a 3D model. Obtained results were validated with experimental data, which show acceptable percentages of error. This work can help design engineers to calculate the operational properties and features of the induction machine with a high reliability and without the need to build a previous prototype.

Nomenclature

3D = Three dimensions
2D = Two dimensions
FEM = Finite Element Method
N_s = Synchronous speed
s = Slip
Nm = Mechanical speed
f_r = Slip frequency
f_e = Electrical frequency

R1 = Resistance of stator
R'2 = Resistance of rotor
Rc = Equivalent resistance to magnetic loss
L1 = Inductance of stator
L'2 = Inductance of rotor
Lm = Inductance of magnetization
$\Re_i$ = Reluctance of silicon steel laminated core
$\Re_a$ = Reluctance of air
φ = Magnetic flux
r = Radial longitude of the laminated core
b = Axial length of the laminated core
μ_i = Permeability of laminated core
μ_0 = Permeability of the air
μ_{eq} = Equivalent permeability of the whole core
L_{er} = Equivalent inductance of rotor
R_{er} = Equivalent resistance of rotor
E = Vector of electric field strength,
B = Vector of magnetic induction,
H = Vector of magnetic field intensity
D = Vector of electric displacement or electric induction
J = Vector of electric current density
ε = Electrical permittivity of the material
σ = Electric conductivity of the material
μ = Magnetic permeability of the material
A = Magnetic vector potential
V = Electric scalar potential
A(x,y) or A_z = Magnetic potential in axial direction
J(x,y)= Current density in axial direction
V_m = Potential in solid conductor
R_m = Resistance in solid conductor
I_m = Current in solid conductor
S = Cross-section of the conductor
Γ = length of the conductor
V_f = Potential in filamentary conductor
I_f = Current in filamentary conductor
R_f = Resistance in filamentary conductor
Nc = Number of turns of the filamentary conductor

References

Altair, F. I. (2016). User guide. CAD package for electromagnetic and thermal analysis using finite elements. France. November 18.

Bastos, J. P. & Sadowski, N. (2003). *Electromagnetic modeling by finite element methods*. Florianopolis: CRC press.

Bertotti, G. (1998). *Hysteresis in magnetism: For physicists, materials scientists and engineers*. Torino: Academic press.

Boldea, I. (2020). *Induction machines handbook*. Boca raton: CRC press.

Castañeda, R., Díaz, A., Domínguez, A. F. & Martínez, C. I. (2020). Soluciones de ecuaciones diferenciales por elemento finito. *Ingeniería, Investigación y Tecnología*, 21 (01), 1-11. https://doi.org/10.22201/fi.25940732e.2020.21n1.002

Cha, J. M., Son, R. W., Yoo, G. H. & Jeon, M. J. (2017). A method of determining the equivalent core length of the large synchronous motor with radial air ducts. *IEEE Transactions on Magnetics*, 1-4.

Escarela, R., Melgoza, E. & Alvarez, J. (2009). Coupling circuit systems and finite element models: A 2-D time-harmonic modified nodal analysis framework. *IEEE transactions on magnetics*, 707-715. http://dx.doi.org/10.1109/TMAG.2008.2010041

Fireţeanu, V., Constantin A. I. & Zorig, A. (2019). Finite element 2D and 3D models of a rotor bar breakage in a squirrel-cage induction motor. Workshop on Electrical Machines Design, Control and Diagnosis, 157-162. Athens: IEEE.

Frosini, L. & Pastura, M. (2020). Analysis and design of innovative magnetic wedges for high efficiency permanent magnet synchronous machines. *Energies*, 13(01), 255. https://doi.org/10.3390/en13010255

Guzmán, J., González-Montañez, F., Escarela-Pérez, R., Olivares-Galván, J. C. & Jiménez-Mondragón, V. M. (2015). Numerical modeling of the thomson ring in stationary levitation using FEM-Electrical network and Newton-Raphson. *Ingeniería, Investigación y Tecnología*, 16(3), 431-439. http://doi.org/10.1016/j.riit.2015.05.005

IEC. (2007). Rotating electrical machines-Part 2-1: Standard methods for determining losses and efficiency from tests (excluding machines for traction vehicles). IEC 60034-2-1., 1-20.

IEEE. (2004). IEEE Standard test procedure for polyphase induction motors and generators. Institute of Electrical and Electronics Engineers, 1-20.

Jimenez, V. M., Escarela, R., Melgoza, E., Arjona, M. A. & Olivares, J. C. (2016). Nonlinear time-harmonic analysis of multiple magnetic field systems: Cartesian, axisymmetric, and coupled circuits. *IEEE Transactions on Magnetics*, 52(10), 1-10.

Kumar, R., Kumar, P., Kanekawa, T. & Oishi, K. (2020). Stray loss model for induction motors with using equivalent circuit parameters. *IEEE Transactions on Energy Conversion*, 1036-1045. http://doi.org/10.1109/tec.2020.2964616

Liu, H. T., Schneider, J., Li, H. L., Sun, Y., Gao, F., Lu, H. H. & Wang, G. D. (2015). Fabrication of high permeability non-oriented electrical steels by increasing< 0 0 1> recrystallization texture using compacted strip casting processes. *Journal of Magnetism and Magnetic Materials*, 577-586.

Pechlivanidou, M. C., Chasiotis, I. D. & Karnavas, Y. L. (2019). A comparative study on 2D and 3D magnetic field analysis of permanent magnet synchronous motor using FEM simulations. *Journal of Electromagnetic Waves and Applications*, 33(17), 2215-2241. https://doi.org/10.1080/09205071.2019.1674190

Pyrhonen, J. A. (2013). *Design of rotating electrical machine*. West Sussex: John Wiley & Sons.

Qiu, H., Wang, S., Sun, F. & Wang, Z. (2020). Transient electromagnetic field analysis for the single-stage fast linear transfor-

mer driver with two different configurations using the finite-element method and finite integration technique. *IEEE Transactions on Magnetics*, 1-14. https://doi.org/10.1109/tmag.2019.2956212

Salon, S. & Chari, M. V. (1999). *Numerical methods in electromagnetism.* New York: Elsevier.

Schuhmann, T., Conradi, A., Deeg, C. & Brandl, K. (2013). Determination of stator end winding inductance of large induction machines: Comparison between analytics, numerics, and measurements. *Electric Power Components and Systems*, 41(14), 1397-1414. https://doi.org/10.1080/15325008.2013.821690

Tong, W., Wu, S. & Tang, R. (2018). Totally enclosed self-circulation axial ventilation system design and thermal analysis of a 1.65-MW direct-drive PMSM. *IEEE Transactions on Industrial Electronics*, 9388-9398. https://doi.org/10.1109/TIE.2018.2823698

Umans, S. D. (2014). *Fitzgerald & Kingsley's electric machinery*. Massachusetts: McGrew-Hill .

Verucchi, C., Ruschetti, C., Giraldo, E., Bossio, G. & Bossio, J. (2017). Efficiency optimization in small induction motors using magnetic slot wedges. *Electric Power Systems Research*, 152, 1-8.

Wang, H., Bao, X., Di, C., Cheng, Z. & Fang, Y. (2014). Current analysis in end ring of submersible motor by finite-element method. Fourth International Conference on Instrumentation and Measurement, Computer, Communication and Control, 983-987 Heilongjiang, IEEE.

Yang, Z., Wang, S., Sun, Y. & Cao, H. (2020). Vibration reduction by magnetic slot wedge for rotating armature permanent magnet motors. *IEEE Transactions on Industry Applications*, 4882-4888. https://doi.org/10.1109/ICEMS.2019.8921662

Cómo citar: Aragon-Verduzco D. A., Escarela-Perez R., Olivares-Galvan J. C., Campero-Littlewood E., Maximov S. & Hernández-Ávila J. L. (2021). Numerical simulation of a squirrel cage motor including magnetic wedges and radial vents. *Ingeniería Investigación y Tecnología*, 22 (04), 1-10. https://doi.org/10.22201/fi.25940732e.2021.22.4.025